










The impact of local pinning sites in magnetic tunnel junctions with non-homogeneous free layers

Alex. S. Jenkins ¹, Leandro Martins¹, Luana C. Benetti ¹, Alejandro Schulman ¹, Pedro Anacleto ¹, Marcel S. Claro ¹, Ihsan Caha¹, Francis Leonard Deepak ¹, Elvira Paz ¹ & Ricardo Ferreira ¹

Pinning at local defects is a significant road block for the successful implementation of technological paradigms which rely on the dynamic properties of non-trivial magnetic textures. Here, a comprehensive study of the influence of local pinning sites for non-homogeneous magnetic layers integrated as the free layer of a magnetic tunnel junction is presented, both experimentally and with corresponding micromagnetic simulations. The pinning sites are found to be extremely detrimental to the frequency controllability of the devices, a key requirement for their use as synapses in a frequency multiplexed artificial neural networks. In addition to describing the impact of the local pinning sites in the more conventional NiFe, a vortex-based magnetic tunnel junction with an amorphous free layer is presented which shows significantly improved frequency selectivity, marking a clear direction for the design of future low power devices.

¹International Iberian Nanotechnology Laboratory, INL, Av. Mestre José Veiga s/n, 4715-330 Braga, Portugal. email: alex.jenkins@inl.int

Defect-induced pinning has long been perceived as a significant challenge for the real-world implementation of many potential applications which aim to harness the dynamical behaviour of complex magnetic textures, the prime example being the so-called ‘racetrack memory’^{1,2}, where local pinning strongly affects the mobility of the magnetic texture under investigation³. Whilst significant study has focussed on the impact on defects on the mobility of domain walls^{4–6} and skyrmions^{7–9} in nanowire configurations, there remains much less understanding of the effect of pinning in magnetic tunnel junctions with free layers that have a non-homogeneous magnetisation. The most common type of non-homogeneous magnetisation texture found in nano-pillars is the magnetic vortex¹⁰, where the exchange and dipolar interactions result in the in-plane magnetisation forming decreasingly small loops, before becoming out-of-plane at the central vortex core. Vortex-based magnetic tunnel junctions (vMTJ) can be simplistically considered as comprising of three layers, a fixed magnetic layer whose magnetisation does not change, an insulating tunnelling layer, and a free magnetic layer, whose ground state is the magnetic vortex.

The magnetisation dynamics of magnetic vortices have been shown optically to be strongly dependent on the pinning sites created by structural defects in polycrystalline NiFe nano-disks^{11–17}, however, there remains limited electrical characterisation of vortex-based magnetic tunnel junctions. Exploring the influence of the pinning of non-trivial magnetisation textures electrically is a crucial step for the realisation of many of the proposed applications which are based on vMTJs, and to this end the spin-diode effect is a valuable characterisation technique capable of analysing the resonant frequency of MTJs by simply applying an rf current and measuring the dc voltage.

Recently, the dynamic properties of MTJs have been attracting significant interest in the context of designing complex neuro-morphic architectures^{18–20}, where vMTJs are the most promising current spintronic technology for such a network due to their relatively high performance as both the dc to rf and rf to dc transducers required for the neuronal and synaptic elements. Although the long term vision of such a system would probably target operational frequencies beyond those found in the vMTJs (typically around 0.1 to 1 GHz), vMTJs are currently the most robust, reproducible and reliable dynamic MTJ technology, and are an attractive candidate for preliminary testing of such networks in hybrid spintronics/CMOS spin chips.

This report focusses on vMTJs in the context of vortex-based frequency selective rectifiers^{21,22}, where individual nano-devices operate as tunable rf to dc transducers, with each device operating at a specific frequency, allowing for a frequency multiplexing approach, which can be utilised in designing complex neuro-morphic architectures^{18–20}. The key element in such devices is the ability to precisely control the frequency of operation of each of these nano-rectifiers, which is usually achieved by controlling the geometry of the individual nanopillars.

In this work, we show how the energy landscape induced by defects in polycrystalline magnetic materials causes the magnetic vortex to be pinned, resulting in a clear sub-threshold pinned dynamic behaviour, as well as the super-threshold conventional gyrotropic motion which is more commonly presented in the literature. Furthermore, we show how the sub-threshold dynamics are controlled, not by the device geometry, but by the local energy landscape of the pinning site. One possible solution to the local pinning sites is by utilising a soft amorphous magnetic material, for example CoFeSiB, which is integrated as the free layer of a magnetic tunnel junction with a significantly reduced impact of local pinning sites.

Results and Discussion

Analysing the local pinning through the spin-diode effect. The devices under investigation are magnetic tunnel junctions with a CoFe(2.0)/Ru(0.7)/CoFeB(2.6 nm) synthetic antiferromagnet (SAF) acting as the pinned layer and a CoFeB(2.0)/Ta(0.2)/X composite layer as the free layer separated by a thin MgO(1.0 nm) layer. The soft magnetic material, X, included in the free layer composite is NiFe(7.0 nm) similar to those discussed in detail in ref. ²³, unless otherwise stated. The patterned devices undergo an annealing treatment of 330 °C for 2 hours in a 1 T magnetic field to align the axis of the pinning antiferromagnetic layer and crystallise the MgO. Similar behaviour was observed for devices with diameters ranging from $d = 300$ – 1000 nm.

The spin-torque diode²⁴ effect is a well-established experimental technique for determining the resonant frequency of the dynamic modes in vMTJs^{21,22,25}, where applying a radio-frequency current results in a rectified voltage as the magnetisation response is transduced into an electrical signal via the tunnelling magnetoresistance response.

In Fig. 1a, the absolute value of the rectified spin-diode voltage is presented as a function of the excitation frequency and power for a vMTJ, where the absolute value of the rectified voltage was chosen so as to allow a log colour scale, in order for both the pinned and gyrotropic modes to be visible on the same graph. In reality, the spin diode response often has an approximate anti-Lorentz lineshape²¹, which crosses zero around the central resonant frequency. The black line which increases as a function of power (labelled the pinned mode) is therefore the central frequency of the pinned mode, and is constant over several orders of magnitude of excitation power, but starts to shift to lower frequencies as the power is increased.

The spin-diode presented in Fig. 1a shows the presence of a clear threshold, P_{rf}^{t} (illustrated in the figure with a white line), below which the vortex core is pinned, and above which the core escapes the pinning sites and enters the gyrotropic mode. This type of threshold behaviour is consistent with results which have been previously explored optically on NiFe nano-disks²⁶. The in-plane magnetic field dependence of the dynamic response is plotted in Fig. 1b and c, for excitation frequencies above and below P_{rf}^{t} , (i.e. $P_{\text{rf}} = 10$ and $150 \mu\text{W}$, respectively).

The frequency of the sub-threshold mode can be seen to vary strongly as a function of the in-plane magnetic field, whereas the super-threshold behaviour has a more constant frequency response, at frequencies consistent with the gyrotropic motion of the vortex core published in the literature (e.g. refs. ^{22,27}) and predicted by the modified Thiele equation²⁸.

In fact, the value of the threshold power, P_{rf}^{t} , can be relatively easily determined experimentally and is plotted in Fig. 1d as a function of the in-plane field. A radio-frequency of $f = 115$ MHz is applied to the MTJ, corresponding to the gyrotropic mode of the vortex confined in a $d = 500$ nm nanopillar, and the power at which the measured rectified voltage exceeds a critical value (i.e. $V_{\text{th}} = 0.2$ mV) is determined. The threshold power can be seen to vary significantly (from 8 to $100 \mu\text{W}$), with the value depending strongly on the value of the in-plane magnetic field, and therefore the location of the vortex core.

For the successful implementation of vMTJs as artificial synapses, the frequency needs to be controlled precisely, and the standard mechanism for controlling the frequency of the gyrotropic mode would be by variation of diameter²³. Figure 1 shows that at low powers, the resonant frequency of the vMTJ is not determined by the geometry but rather by the local pinning sites, which means that for the successful realisation of the artificial synapse operating at low rf powers (i.e. $P_{\text{rf}} \sim 1 \mu\text{W}$), the

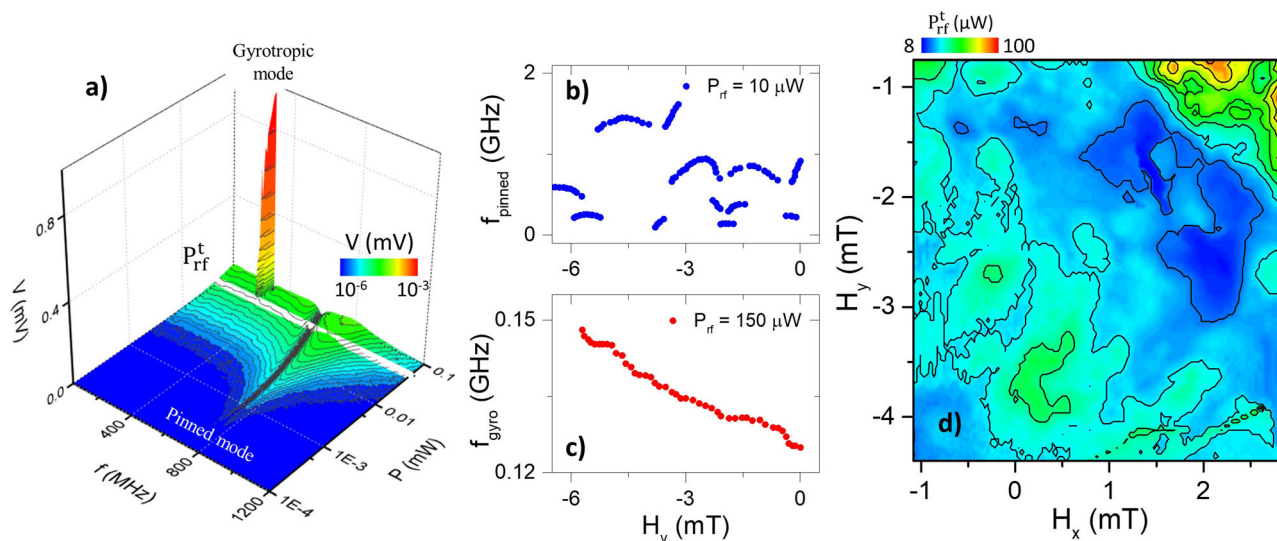


Fig. 1 Influence of pinning on spin-diode measurements. **a** Absolute magnitude of the experimentally determined spin-diode voltage as a function of the excitation frequency and power with the white line showing the threshold power, P_{rf}^t , at which the vortex core escape the pinning site and P_{rf}^t the resonant frequency of **b** the pinned mode ($P_{rf} = 10 \mu\text{W}$) and **c** the gyrotropic mode ($P_{rf} = 150 \mu\text{W}$). **d** The threshold radio-frequency power, P_{rf}^t , as a function of the magnetic field applied along the x- and y-axis for an excitation current of $f_{gyro} = 115 \text{ MHz}$.

threshold for escaping the pinning site needs to be substantially reduced.

In addition to affecting the gyrotropic mode of the vortex core, the grains also affect the higher order spin wave modes, which can also be probed via the spin-diode effect²⁵. It has been suggested previously that defects can alter the nature of these higher order spin-wave modes^{29,30}. In Supplementary Figure 1, the spin-diode for the spin wave modes is presented, where it can be seen that there is a slight variation in the modes as a function of the pinning site, but less than experienced for the gyrotropic mode.

Micromagnetic simulations of the energy landscape. Micromagnetic simulations can be utilised to better illustrate difference between the sub-threshold pinned dynamics and the super-threshold conventional gyrotropic mode. The micromagnetic simulations were performed using the mumax3 code³¹ for 500 nm nanopillars with typical NiFe material parameters ($M_{sat} = 740 \times 10^3 \text{ A/m}$, $A_{ex} = 1.3 \times 10^{-11} \text{ J/m}$, $\alpha = 0.01$). Although the pinning defects could be caused by other means (i.e. roughness¹⁴), in these simulations the local pinning defects were introduced by creating a random granular structure¹⁷. The nanopillar was separated into individual grains with an average size of 20 nm (values of the grain size in NiFe in the literature vary between 4 and 10 nm in ref. ¹⁷, 35 and 85 nm in ref. ¹¹, 30 nm in ref. ¹³). The lower end of the range of grains sizes was selected as the free layer in this study is relatively thin ($t_{NiFe} = 7 \text{ nm}$) and the grain size tends to increase with thickness¹⁴. Local pinning sites were created by randomly varying the saturation magnetisation of the grains between M_{sat} and $0.85 \cdot M_{sat}$ and the inter-region exchange at the boundaries between the grains was also reduced to $0.85 \cdot A_{ex}$ at the granular interface.

In Fig. 2, the energy landscape has been plotted as a function of the x and y position within the nanopillar. The simulations were performed by initialising a magnetic vortex at different lateral positions (i.e., x and y) and waiting for a short time period (i.e. $\sim 0.1 \text{ ns}$) for the core to stabilise and calculating the subsequent energy, which comprises of the demagnetising, exchange and Zeeman component energy terms. In Fig. 2a, the energy of the whole of the nanopillar is calculated, and results in a standard

parabolic potential minima. Although the granular defects are very slightly visible, the majority of the energy landscape is dominated by the edges of the nanopillar, with the in-plane part of the magnetic vortex typically being > 500 times in size compared to the vortex core.

In Fig. 2b, however, the energy landscape is again calculated, except this time only the energy within an area comparable to the vortex core (i.e. a circle with radius $r = 16 \text{ nm}$) is calculated, and the local energy minima felt by the vortex core is presented. The impact of the granular defects is now much more pronounced, with lots of local maxima and minima visible. To illustrate the sub-threshold and super-threshold dynamics, typical trajectories of the vortex core when strongly pinned and after escaping the pinning site (i.e. the gyrotropic mode) are plotted.

In order to validate the micromagnetic simulations with the experimental data in the sub-threshold regime, in Fig. 3, the frequency of the pinned mode is determined as a function of the in-plane magnetic field (both transverse and along the MTJ easy axis, i.e. H_x and H_y respectively). The frequency was determined via FFT analysis of the magnetisation aligned along the easy-axis in the micromagnetic simulations, i.e. the m_y component, as the magnetic vortex relaxes over 50 ns. As the magnetic vortex relaxes towards equilibrium, a clear peak in frequency can be detected in the FFT of the m_y component, which is considered to be the relaxation frequency of the vortex in the pinned state. In Fig. 3, this data is compared to the experimentally determined resonant frequency for a low, i.e. sub-threshold, excitation power of $P_{rf} = 10 \mu\text{W}$. The experimental resonance frequency is determined by sweeping the low power rf current, and extracting the central frequency of the dc voltage response, corresponding to the resonant frequency.

There is good agreement between the experimentally acquired spin-diode effect and the micromagnetic simulations, with the resonant frequency varying strongly as a function of the in-plane magnetic field, with different regions of similar resonant frequency corresponding to different pinning sites.

To further explore the different pinning sites and their consequent effect on the vortex dynamics, two magnetic fields were identified in Fig. 3b (i.e. $[H_x, H_y] = -4.2, 3.3 \text{ mT}$ and $[H_x, H_y] = -5.4, 2.6 \text{ mT}$, labelled 1 and 2 respectively) with very

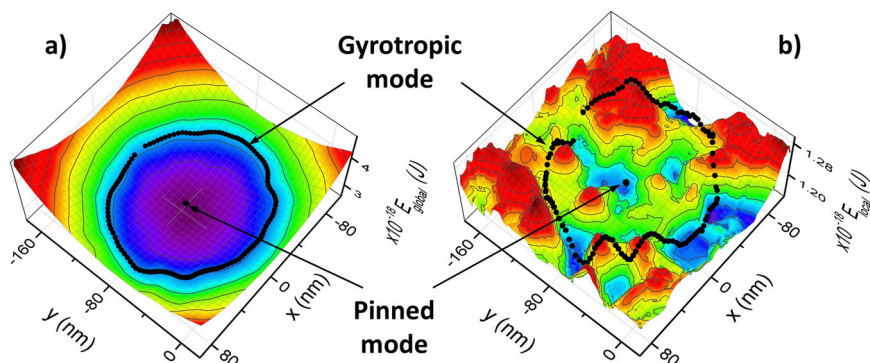


Fig. 2 Energy landscape simulations. Energy landscape calculated with micromagnetic simulations considering **a**) the whole nanopillar and **b**) a 16 nm radius around the vortex core. The black dots shows typical trajectories of the sub-threshold pinned mode and the super-threshold gyrotropic mode.

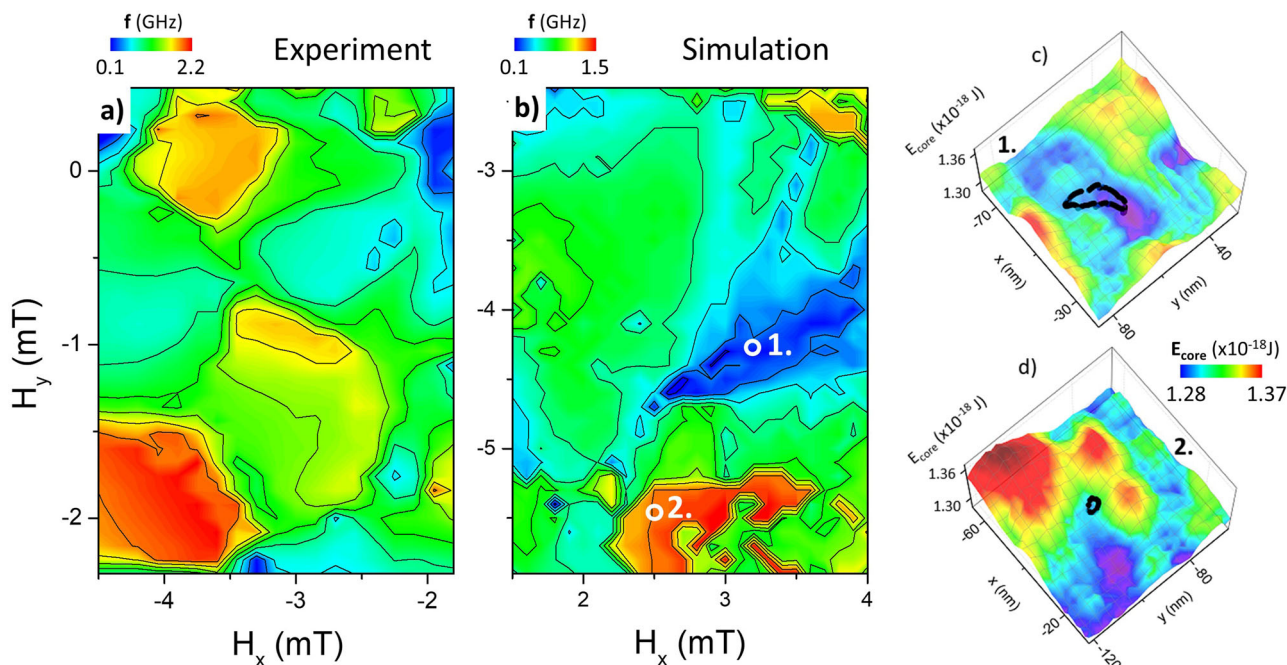


Fig. 3 Frequency variation at different pinning sites. Resonant frequency of the sub-threshold pinned mode as determined **a**) experimentally via spin diode effect and via **b**) micromagnetic simulations, as a function of the in-plane magnetic field (H_x and H_y). Energy landscape as calculated with micromagnetic simulations for two different in-plane magnetic fields i.e. **c**) $H_x = -4.2$ mT and $H_y = 3.3$ and **d**) $H_x = -5.4$ mT and $H_y = 2.6$ mT. The black line corresponds to the trajectory of the vortex core when excited with an rf signal of 1 mA and a frequency of $f_1 = 220$ MHz and $f_2 = 1400$ MHz.

different resonant frequencies ($f_1 = 220$ MHz and $f_2 = 1400$ MHz). These two fields correspond to a weakly pinned system (i.e. position 1) and a strongly pinned system (i.e. position 2). The energy landscapes calculated via micromagnetic simulations of these two different field values are presented in Fig. 3c and d. Additionally, the typical trajectories of the sub-threshold pinned mode are presented for two resonant excitations ($f_1 = 220$ MHz and $f_2 = 1400$ MHz for an excitation current of 1 mA). For position 1, the loosely pinned vortex core has a resonant frequency close to the global gyrotropic frequency, and the core is excited to relatively large orbits. This pinning site is spatially larger and is caused by two grains of relatively low saturation magnetisation being located next to one another (Supplementary Figure 2). In the case of position 2, the strongly pinned core can be resonantly excited by applying a frequency far from the global gyrotropic mode, and results in a relatively small orbit. This energy minima is caused by the intersection of multiple grain boundaries which result in a pronounced yet spatially localised minima (Supplementary Fig. 3). The origin of the pinning site appears to have a pronounced impact

on the vortex core dynamics leading to the possibility that analysis of the resonant frequency of the vortex core and subsequent comparison to micromagnetic simulations may provide an interesting tool for exploration of the granular structure of magnetic materials in the future.

Reducing the influence of pinning with amorphous free layers.

Having identified the challenge posed by local pinning sites in vortex-based magnetic tunnel junctions, we now present two potential solutions for reducing the impact of these local energy minima on the vortex dynamics; removing granular defects by using an amorphous free layer and reducing the impact of the interface by increasing the free layer thickness. The work presented in the first half of this report uses a CoFeB/Ta/NiFe composite free layer, where the polycrystalline NiFe is chosen due to its magnetic softness, and the CoFeB is selected to ensure good texture in the insulating MgO barrier, and therefore subsequent high tunneling magnetoresistance. The CoFeB is amorphous as

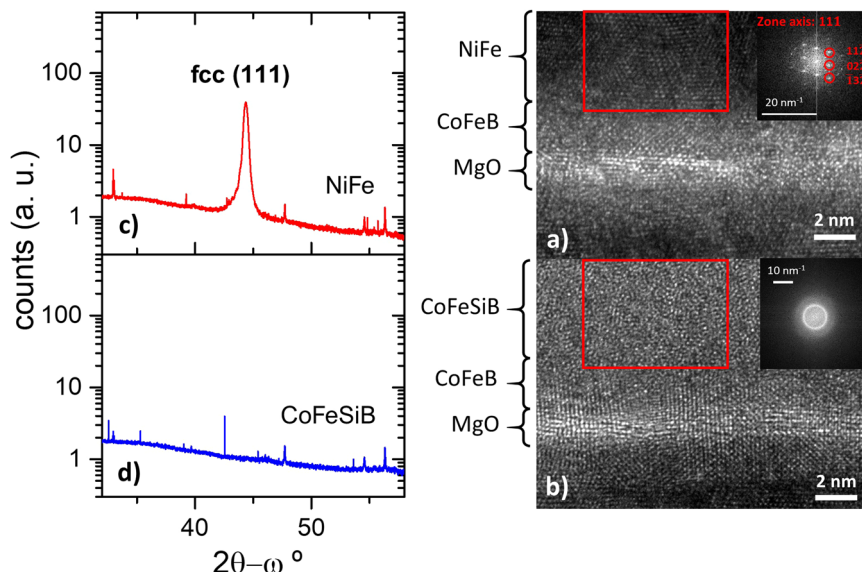


Fig. 4 NiFe and CoFeSiB crystallography comparison. x-ray diffraction pattern of **a)** NiFe and **b)** CoFeSiB annealed thin films as well as cross sectional TEM images of two patterned magnetic tunnel junction devices with **c)** CoFeB/Ta/NiFe and **d)** CoFeB/Ta/CoFeSiB free layers.

deposited, but crystallises into bcc (001) during the annealing which is an essential step to ensure high TMRs above 100%. The Ta layer is to ensure a separation of crystallicity between the NiFe and the CoFeB.

Whilst the CoFeB/Ta/NiFe composite layer has shown good results for large power excitations, the polycrystalline nature of the free layer results in additional pinning sites. In order to avoid this, an amorphous soft magnetic layer has been selected to replace the NiFe, namely CoFeSiB. $\text{Co}_{67}\text{Fe}_{4}\text{Si}_{14.5}\text{B}_{14.5}$ is an interesting candidate for magnetic tunnel junctions as it is amorphous after standard annealing processes³² and has been previously investigated in micron-sized AIO-based magnetic tunnel junctions where lower switching fields were observed^{33–35}. Figure 4a and b shows the x-ray diffraction measurement of two thin films, NiFe and CoFeSiB respectively, after annealing at 330 °C. A clear peak associated with fcc (111) is observed for the polycrystalline NiFe, whereas no peak is observed for the CoFeSiB.

As well as being amorphous in unpatterned thin films, in Fig. 4c and d the cross sectional transmission electron microscopy (TEM) is presented for two patterned magnetic tunnel junction devices, with c) CoFeB/Ta/NiFe and d) CoFeB/Ta/CoFeSiB free layers. By analysis of the Fast Fourier Transform (FFT), the NiFe image is shown to be consistent with a orthorhombic crystal with 111 zone axis, whilst the CoFeSiB appears amorphous after patterning and annealing.

Having identified CoFeSiB as an amorphous free layer, even after annealing, nano-devices were patterned and their resonant frequency was investigated via the spin diode effect (similar to Fig. 1b) with an rf current of $P_{\text{rf}} = 1 \mu\text{W}$. As seen in Fig. 5a, the CoFeB(2.0)/Ta(0.5)/NiFe(7.0 nm) shows the sub-threshold behaviour discussed in Fig. 1, with a drastic variation of the resonant frequency as a function of the in-plane magnetic field, as the core moves from one pinning site to another, each with markedly different energy landscapes and therefore resonant frequencies. When the NiFe is replaced with CoFeSiB(7 nm), shown in Fig. 5b, the resonant frequency is seen to still vary significantly as a function of the in-plane magnetic field but with the impact being reduced by the amorphous nature of the CoFeSiB. Whilst there still exists a variation in frequency, this can be seen to be between 0.1 – 1 GHz (relative to the 0.1 – 2.5 GHz of the NiFe), the fact

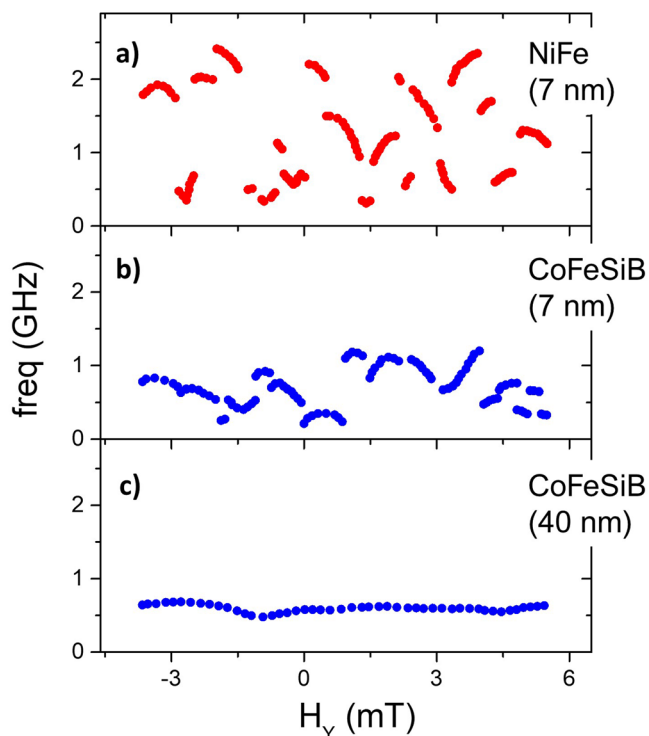


Fig. 5 Frequency variation reduction in amorphous free layers. The measured resonant frequency as a function of the in-plane magnetic field for the magnetic tunnel junctions of 400 nm diameter, with a free layer comprised of **a)** CoFeB(2.0)/Ta(0.5)/NiFe(7 nm), **b)** CoFeB(2.0)/Ta(0.5)/CoFeSiB(7 nm) and **c)** CoFeB(2.0)/Ta(0.5)/CoFeSiB(40 nm).

that the vortex continues to be in the sub-threshold pinned regime even with an amorphous free layer suggests that the impact of interfacial roughness and the polycrystalline CoFeB are still playing an important role in the energy landscape. In Fig. 5c, the thickness of the CoFeSiB is increased to 40 nm and the variation in resonant frequency can be seen to drastically reduce, with the spin diode response being observed mostly between 0.5

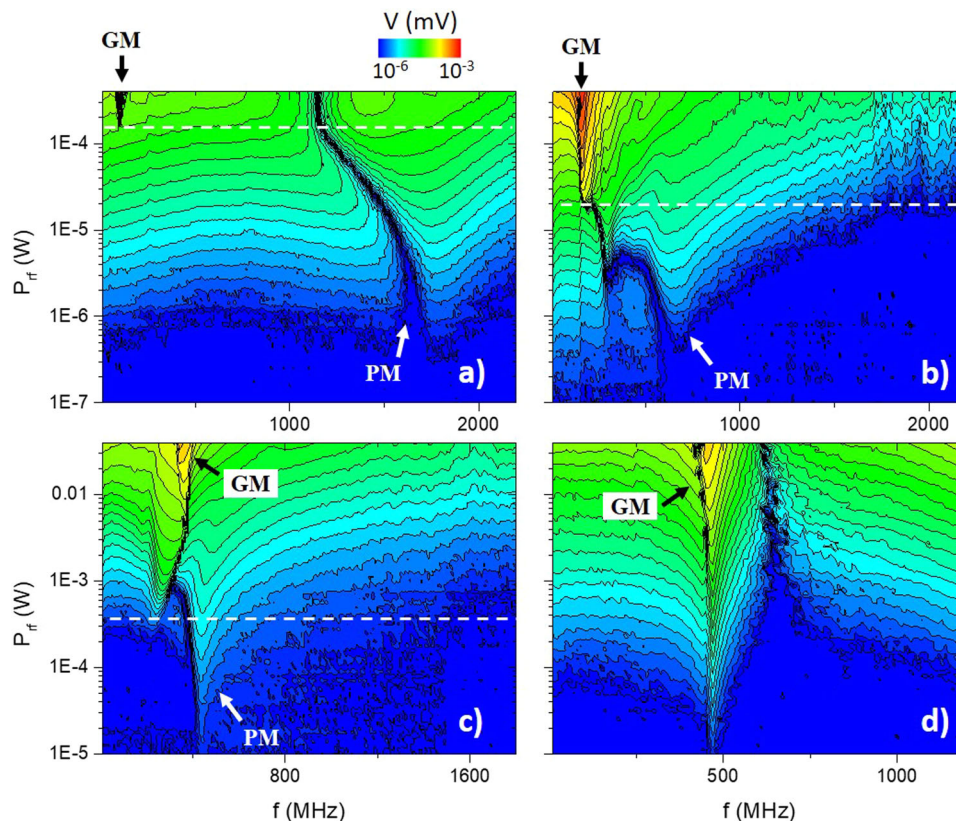


Fig. 6 Pinning threshold reduction with CoFeSiB thickness. **a)** Absolute magnitude of the experimentally determined spin-diode voltage as a function of the excitation frequency and power with the white line showing the threshold power, P_{rf}^t , at which the vortex core escape the pinning site for a free layer of CoFeB(2.0)/Ta(0.5)/CoFeSiB(X nm), where $X = \mathbf{a)}$ 3 nm, **b)** 7 nm, **c)** 20 nm and **d)** 40 nm. GM signifies the gyrotropic mode and PM represents the pinned mode.

and 0.6 GHz, demonstrating a substantial reduction of frequency variation due to the local pinning sites.

The reduction of the frequency variation as a function of in-plane magnetic field for the amorphous CoFeSiB free layer is important in the context of rf-based artificial synapses, but the significance goes beyond this particular case, and has more wide-ranging implications. The frequency variation can be considered as a measurement of the pinning sites and, therefore, the thick amorphous CoFeSiB shows reduced pinning in general, making it an interesting candidate for further study for a range of technological implementations, for example, racetrack memory or magnetic field sensors. Further study is needed to accurately extract the material parameters of CoFeSiB (e.g. damping and exchange constant), and one potential drawback with using such thick free layer materials is that the critical current for steady state oscillations will depend on the thickness of the material²⁸, so that observing the dc to rf transduction may not be possible with such thick layers.

To further explore the reduction in pinning for thicker CoFeSiB, in Fig. 6 the absolute value of the rectified spin diode voltage measured at zero applied magnetic field is presented as a function of the rf power and frequency (equivalent to Fig. 1a), for four different CoFeSiB thicknesses. The free layer consists of CoFeB(2.0)/Ta(0.5)/CoFeSiB(X nm), where $X = 3, 7, 20$ and 40 nm for a, b, c and d, respectively. For the thinnest CoFeSiB, the pinning threshold is around $P_{rf} = 100 \mu\text{W}$, similar to that observed in NiFe (although this threshold varies strongly as a function of the local pinning sites). This threshold reduces to around 20 mW and 4 mW for $X = 7$ and 20 nm respectively. For the case of $X = 40$ nm, there is no clear threshold visible and the

gyrotropic mode is accessible even down to $P_{rf} = 100$ nW, which is therefore a gain of around three order of magnitude over the relatively thinner $X = 3$ nm.

Conclusion

In conclusion, the impact of local pinning sites is explored in vortex-based magnetic tunnel junctions, where the pinning of the magnetic vortex core results in a threshold in the excitation power, which must be overcome before large orbit gyrotropic motion is observed. In these pinned states, the resonant frequency of the nano-device is strongly impacted by the local energy landscape leading to a drastic variation in the resonant frequency. These pinning sites represent a significant challenge for the implementation of vortex-based frequency selective rectifiers, however by using an amorphous free layer, namely CoFeSiB, the impact of the vortex core pinning is significantly reduced. The integration of amorphous materials as the free layer of magnetic tunnel junctions with non-trivial magnetic textures offers a potentially ‘pinning-free’ system, which can dramatically improve device performance in the low-power regime.

Methods

Device Fabrication. The NiFe-based magnetic tunnel junctions have the following stack 6.0 IrMn/2.0 CoFe30/0.7 Ru/2.6 CoFe40B20/0.8 MgO/2.0 CoFe40B20/0.2 Ta/7.0 NiFe (thickness in nanometers), and for the devices identified as the CoFeSiB, the NiFe was replaced with $\text{Co}_{67}\text{Fe}_4\text{Si}_{14.5}\text{B}_{14.5}$. The devices were patterned using ebeam and optical lithography techniques and are annealed at 330 °C for 2 hours in a 1 T magnetic field to align the

axis of the pinning antiferromagnetic layer and crystallise the MgO.

Spin-diode measurements. The spin-diode measurements were performed by using a standard bias tee, with a voltmeter connected to the dc port and an rf source connected to the ac port. The in-plane magnetic field was swept either with a solenoid or by applying a dc current to an integrated field line located directly above the MTJ which can create a local in-plane magnetic field.

Transmission electron microscopy. Transmission electron microscopy (TEM) imaging of the samples were carried out with a double corrected FEI Titan G3 Cubed Themis equipped with a Super-X EDX detector, operated at 200 kV. The samples for TEM analysis were prepared by a dual-beam FEI Helios focused ion beam (FIB) following the standard lift-out procedure. In order to not destroy the formed oxide layer on the samples by Ga⁺ ions during the milling steps, two Pt layers were deposited: ~200 nm by electron (e⁻) beam and ~2 μm by ion (i⁻) beam. 30 kV ion beam was used for the bulk milling, and thereafter the lamella was thinned down to 100 nm in thickness. Finally, a 5 kV ion beam was used to remove the surface amorphization layer.

Data availability

The data supporting this scientific work are available from the corresponding author upon reasonable request.

Received: 14 April 2023; Accepted: 2 November 2023;

Published online: 16 January 2024

References

- Parkin, S. S. P., Hayashi, M. & Thomas, L. Magnetic domain-wall racetrack memory. *Science* (80-) **320**, 190 (2008).
- Fert, A., Cros, V. & Sampaio, J. Skyrmions on the track. *Nat. Nanotechnol.* **8**, 152–156 (2013).
- Thiaville, A., Nakatani, Y., Miltat, J. & Suzuki, Y. Micromagnetic understanding of current-driven domain wall motion in patterned nanowires. *Europhys. Lett.* **69**, 990 (2005).
- Meier, G. et al. Direct imaging of stochastic domain-wall motion driven by nanosecond current pulses. *Phys. Rev. Lett.* **98**, 187202 (2007).
- Lemerle, S. et al. Domain Wall Creep in an Ising Ultrathin Magnetic Film. *Phys. Rev. Lett.* **80**, 849 (1998).
- Leliaert, J. et al. Influence of material defects on current-driven vortex domain wall mobility. *Phys. Rev. B - Condens. Matter Mater. Phys.* **89**, 064419 (2014).
- Müller, J. & Rosch, A. Capturing of a magnetic skyrmion with a hole. *Phys. Rev. B - Condens. Matter Mater. Phys.* **91**, 054410 (2015).
- Legrand, W. et al. Room-Temperature Current-Induced Generation and Motion of sub-100 nm Skyrmions. *Nano Lett.* **17**, 2703 (2017).
- Salimath, A., About, A., Brataas, A. & Manchon, A. Current-driven skyrmion depinning in magnetic granular films. *Phys. Rev. B* **99**, 104416 (2019).
- Dussaux, A. et al. Large microwave generation from current-driven magnetic vortex oscillators in magnetic tunnel junctions. *Nat. Commun.* **1**, 1 (2010).
- Compton, R. L. & Crowell, P. A. Dynamics of a pinned magnetic vortex. *Phys. Rev. Lett.* **97**, 137202 (2006).
- Compton, R. L., Chen, T. Y. & Crowell, P. A. Magnetic vortex dynamics in the presence of pinning. *Phys. Rev. B - Condens. Matter Mater. Phys.* **81**, 144412 (2010).
- Kim, J. S. et al. Current-induced vortex dynamics and pinning potentials probed by homodyne detection. *Phys. Rev. B - Condens. Matter Mater. Phys.* **82**, 104427 (2010).
- Chen, T. Y., Erickson, M. J., Crowell, P. A. & Leighton, C. Surface roughness dominated pinning mechanism of magnetic vortices in soft ferromagnetic films. *Phys. Rev. Lett.* **109**, 097202 (2012).
- Burgess, J. A. J. et al. Quantitative magneto-mechanical detection and control of the Barkhausen effect. *Science* (80-) **339**, 1051 (2013).
- Burgess, J. A. J., Losby, J. E. & Freeman, M. R. An analytical model for vortex core pinning in a micromagnetic disk. *J. Magn. Magn. Mater.* **361**, 140 (2014).
- Möller, M., Gaida, J. H. & Ropers, C. Pinning and gyration dynamics of magnetic vortices revealed by correlative Lorentz and bright-field imaging. *Phys. Rev. Res.* **4**, 013027 (2022).
- Leroux, N. et al. Hardware realization of the multiply and accumulate operation on radio-frequency signals with magnetic tunnel junctions. *Neuromorphic Comput. Eng.* **1**, 011001 (2021).
- Leroux, N. et al. Radio-Frequency Multiply-and-Accumulate Operations with Spintronic Synapses. *Phys. Rev. Appl.* **15**, 034067 (2021).
- Ross, A. et al. Multilayer spintronic neural networks with radiofrequency connections. *Nat. Nanotechnol.* **2023**, 1 (2023).
- Martins, L. et al. Non-volatile artificial synapse based on a vortex nano-oscillator. *Sci. Reports* **11**, 1 (2021). 2021 111.
- Marković, D. et al. Detection of the Microwave Emission from a Spin-Torque Oscillator by a Spin Diode. *Phys. Rev. Appl.* **13**, 044050 (2020).
- Jenkins, A. S. et al. Wideband High-Resolution Frequency-to-Resistance Converter Based on Nonhomogeneous Magnetic-State Transitions. *Phys. Rev. Appl.* **13**, 014046 (2020).
- Tulapurkar, A. A. et al. Spin-torque diode effect in magnetic tunnel junctions. *Nature* **438**, 339 (2005).
- Jenkins, A. S. et al. Electrical characterisation of higher order spin wave modes in vortex-based magnetic tunnel junctions. *Commun. Phys.* **4**, 1 (2021). 2021 41.
- Chen, T. Y., Galkiewicz, A. T. & Crowell, P. A. Phase diagram of magnetic vortex dynamics. *Phys. Rev. B* **85**, 180406 (2012).
- Tsunegi, S., Yakushiji, K., Fukushima, A., Yuasa, S. & Kubota, H. Microwave emission power exceeding 10 μW in spin torque vortex oscillator. *Appl. Phys. Lett.* **109**, 252402 (2016).
- Dussaux, A. et al. Field dependence of spin-transfer-induced vortex dynamics in the nonlinear regime. *Phys. Rev.* **014402**, 1 (2012).
- Winters, D., Abeed, M. A., Sahoo, S., Barman, A. & Bandyopadhyay, S. Reliability of Magnetoelastic Switching of Nonideal Nanomagnets with Defects: A Case Study for the Viability of Straintronic Logic and Memory. *Phys. Rev. Appl.* **12**, 034010 (2019).
- Abeed, M. A., Sahoo, S., Winters, D., Barman, A. & Bandyopadhyay, S. The effect of material defects on resonant spin wave modes in a nanomagnet. *Sci. Reports* **9**, 16635 (2019).
- Vansteenkiste, A. et al. The design and verification of MuMax3. *AIP Adv.* **4**, 107133 (2014).
- Celegato, F., Coïsson, M., Olivetti, E., Tiberto, P. & Vinai, F. A study of magnetic properties in CoFeSiB amorphous thin films submitted to furnace annealing. *Phys. Status Solidi* **205**, 1745 (2008).
- Kim, Y. K. Magnetic tunnel junctions comprising amorphous NiFeSiB and CoFeSiB free layers. *J. Magn. Magn. Mater.* **304**, 79 (2006).
- Löhndorf, M., Dokupil, S., Wecker, J., Rührig, M. & Quandt, E. Characterization of magnetic tunnel junctions (MTJ) with magnetostrictive free layer materials. *J. Magn. Magn. Mater.* **272–276**, 2023 (2004).
- Hwang, J. Y. et al. Switching characteristics of magnetic tunnel junction with amorphous CoFeSiB free layer. *J. Magn. Magn. Mater.* **304**, e276 (2006).

Acknowledgements

This work has received funding from the European Union's Horizon 2020 research and innovation programme under grant agreement No 101017098 (project RadioSpin), No 899559 (project SpinAge) and No 101070287 (project Swan-on-chip).

Author contributions

A.S.J., R.F., L.C.B., A.S., L.M. prepared the manuscript. Devices were fabricated and optimised by L.C.B., A.S., P.A., E.P., M.C., L.M. and the TEM was performed by I.C. and L.D.F. and spin diode measurements were performed by A.S.J. and L.M. and A.S.J. was responsible for the micromagnetic simulations.

Competing interests

The authors declare no competing interests.

Additional information

Supplementary information The online version contains supplementary material available at <https://doi.org/10.1038/s43246-023-00423-x>.

Correspondence and requests for materials should be addressed to Alex. S. Jenkins.

Peer review information *Communications Materials* thanks Muhammad Naqi, Jesse Berezovsky and the other, anonymous, reviewer(s) for their contribution to the peer review of this work. Primary Handling Editor: Aldo Isidori. A peer review file is available.

Reprints and permission information is available at <http://www.nature.com/reprints>

Publisher's note Springer Nature remains neutral with regard to jurisdictional claims in published maps and institutional affiliations.



Open Access This article is licensed under a Creative Commons Attribution 4.0 International License, which permits use, sharing, adaptation, distribution and reproduction in any medium or format, as long as you give appropriate credit to the original author(s) and the source, provide a link to the Creative Commons license, and indicate if changes were made. The images or other third party material in this article are included in the article's Creative Commons license, unless indicated otherwise in a credit line to the material. If material is not included in the article's Creative Commons license and your intended use is not permitted by statutory regulation or exceeds the permitted use, you will need to obtain permission directly from the copyright holder. To view a copy of this license, visit <http://creativecommons.org/licenses/by/4.0/>.

© The Author(s) 2024